Applications of quartz tuning forks in spectroscopic gas sensing

Anatoliy A. Kosterev[a] and Frank K. Tittel
Rice Quantum Institute, Rice University, Houston, Texas 77251-1892

Dmitry V. Serebryakov, Alexander L. Malinovsky, and Igor V. Morozov
Institute of Spectroscopy RAS, Troitsk, Russia

(Received 25 October 2004; accepted 7 February 2005; published online 23 March 2005)

A recently introduced approach to photoacoustic detection of trace gases utilizing a quartz tuning fork (TF) as a resonant acoustic transducer is described in detail. Advantages of the technique called quartz-enhanced photoacoustic spectroscopy (QEPAS) compared to conventional resonant photoacoustic spectroscopy include QEPAS sensor immunity to environmental acoustic noise, a simple absorption detection module design, and its capability to analyze gas samples ~ 1 mm^3 in volume. Noise sources and the TF properties as a function of the sampled gas pressure, temperature and chemical composition are analyzed. Previously published results for QEPAS based chemical gas sensing are summarized. The achieved sensitivity of 5.4×10^{-9} cm^{-1} W/$\sqrt{\text{Hz}}$ is compared to recent published results of photoacoustic gas sensing by other research groups. An experimental study of the long-term stability of a QEPAS-based ammonia sensor is presented. The results of this study indicate that the sensor exhibits very low drift, which allows data averaging over >3 h of continuous concentration measurements. Architecture and practical implementation of autonomous QEPAS-sensor controller electronics is described. Future developments of QEPAS technique are outlined. © *2005 American Institute of Physics.* [DOI: 10.1063/1.1884196]

I. INTRODUCTION

The detection and quantification of trace chemical species in the gas phase find applications in such diverse fields as in environmental monitoring, industrial process control, and medical diagnostics. Ultrasensitive chemical analysis of gases based on molecular absorption in the mid-IR region is a well-established approach.[1] A number of techniques have been developed to measure absorption coefficients as low as $\alpha=10^{-9}$ cm^{-1} or less, allowing in some cases quantification of chemical species at 10^{-12} by volume (pptv) concentration levels. However, most methods demonstrated in the laboratory are unsuitable for real world applications because of the sensor size, weight, power consumption and high sensitivity to vibrations and temperature variations.

Recent advances in quantum electronics resulted in compact, efficient and powerful infrared laser sources. Commercially available single-frequency fiber-coupled diode lasers can emit up to 100 mW cw power in the near-IR (molecular overtones) region. Their industrial-grade packaging allows direct integration of such semiconductor sources into portable gas sensors. Fiber amplifiers can boost the optical power of diode lasers to the several watts level. Quantum cascade lasers[2] and interband cascade lasers[3] are capable of generating tens to hundreds of mWs of optical radiation in the molecular fingerprint (mid-IR) region. In order to take full advantage of these achievements for spectroscopic chemical sensing, detection techniques should be used that benefit from high power of these now-available infrared laser sources. Furthermore, the absorbance detection module (ADM) should preferably match the laser source in size and be immune to the environmental factors.

Typically, an ADM for sensitive direct absorption spectroscopy consists of a multi-pass absorption cell and an optical detector. The characteristic optical multi-pass gas cell volume is ~ 1000 cm^3, and this approach does not essentially gain from high optical power because of the limited dynamic range of infrared detectors. Photoacoustic spectroscopy (PAS)[4] can achieve comparable detection limits with a much smaller sample cell volume, typically starting from ~ 10 cm^3.[5] Furthermore, PAS sensitivity is directly proportional to the available laser power. However, PAS performance can be impacted by ambient acoustic noise which prevents its widespread use in the design of portable gas sensors. In this work we describe a recently developed variation of PAS called quartz-enhanced photoacoustic spectroscopy, or QEPAS. This approach allows the analysis of gas samples ~ 1 mm^3 in volume, results in immunity to environmental acoustic noise, and the QEPAS ADM size matches the size of telecommunications diode lasers.

II. FUNDAMENTALS OF QEPAS

When optical radiation is absorbed in a medium such as a gas, it causes heating of the medium that gives rise to thermal expansion. Thus, absorption of modulated radiation results in sound generation. Detection of this optically generated sound with a sensitive microphone is the basis for PAS. In this work we shall consider PAS in gases. To enhance the amplitude of the PA sound, it is common to surround the gas sample with an acoustic resonator.[5] In such a

[a]Author to whom correspondence should be addressed; electronic mail: akoster@rice.edu

configuration the amplitude of the sound wave builds up during $\sim Q$ laser modulation periods, where Q is the Q factor of the acoustic resonator. In the most important case of an optically thin gas layer inside the resonator the detected signal S can be expressed as

$$S = k\frac{\alpha \ell CPQ}{fV} = k\frac{\alpha CPQ}{fA}, \tag{1}$$

where α is the absorption coefficient per unit concentration of the target species, C is the concentration of the target species, P is the optical power, f is the PA sound frequency, V is the resonator volume, A is the resonator cross-section area, and k is a constant describing microphone transfer function and other system parameters. Usually PA resonators are designed for f values in the 500–4000 Hz range and have Q factors of $\sim$20–200.

QEPAS is an alternative way to detect weak PA excitation. The basic idea of QEPAS is to invert the common PAS approach and accumulate the acoustic energy not in a gas-filled cell but in a sharply resonant acoustic transducer. Such an approach removes restrictions imposed on the gas cell by acoustic resonance conditions. The transducer can be positioned in the acoustic near-field zone of the excitation optical beam, in which case the gas enclosure is optional and serves only to separate the gas sample from the environment and control its pressure.

Conventional microphones are not suitable for this task because they are designed for flat frequency response. A natural candidate for such an application is crystal quartz, because it is a widely used low-loss piezoelectric material. A variety of packaged quartz crystals aimed at timing applications is commercially available. Most of them, however, resonate at megahertz frequencies and are therefore not appropriate to gas-phase PAS, because the energy transfer processes in gases occur on a longer time scale, and also because the PA signal decreases at higher frequencies [Eq. (1)]. The only readily available low-frequency quartz elements are quartz tuning forks (TF) intended for use in electronic clocks as frequency standards (Fig. 1, top). TFs resonate at 32 768 (2^{15}) Hz in vacuum. Only the symmetric vibration of a TF (i.e., the two TF prongs bend in opposite directions) is piezoelectrically active. Hence the excitation beam should pass through the gap between the TF prongs for efficient excitation of this vibration.

Acoustically, a quartz TF is a quadrupole, which results in excellent environmental noise immunity. Sound waves from distant acoustic sources tend to move the TF prongs in the same direction, thus resulting in no electrical response. The choice of crystal quartz as an acoustic transducer for the PAS modification explains the acronym QEPAS to denote this technique.

The principal procedure of QEPAS data acquisition is similar to conventional PAS and was described in Ref. 6. The QEPAS studies reported to date were performed using a wavelength modulation approach and $2f$ detection,[7] which suppresses the background originating from spectrally nonselective absorbers (such as resonator walls, TF electrodes, and the gas cell elements). The laser beam is focused between the prongs of the TF and its wavelength is modulated

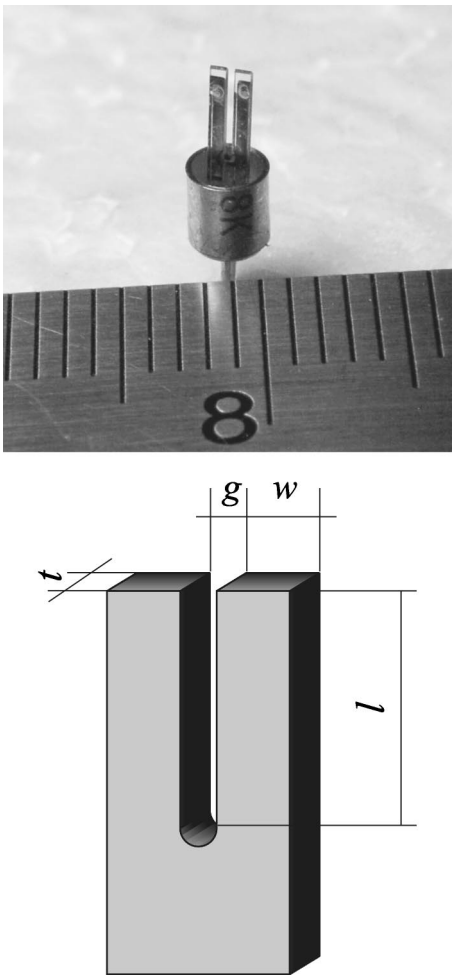

FIG. 1. Photograph of a typical wristwatch TF when top part of the TF housing is removed (top). TF dimensions notation (bottom).

at $f_m = f_0/2$ frequency, where f_0 is the TF resonant frequency. A lock-in amplifier is used to demodulate the TF response at f_0. Spectral data can be acquired if the laser wavelength is scanned. To increase the effective interaction length between the radiation-induced sound and the TF, an acoustic gas-filled resonator may be added similarly as in the traditional PAS approach.

Analogous to conventional PAS, the QEPAS response to optical absorption is described by Eq. (1), where $f = f_0$ is the resonant frequency of the TF. If the TF is used without an additional resonator, A represents an effective cross section which should be approximately equal to the square of the TF gap. The Q is now a parameter of the TF and typically ranges from 10^4 to 10^5, depending on the surrounding gas (see the next section).

The minimum optical absorption coefficient detectable with a PAS based sensor is determined by the condition $S = N$, where S is a PA signal and N is the noise level (which is assumed to be independent of the optical excitation). Usually the noise power density can be considered constant within the detector bandwidth Δf. In this case the average noise magnitude $N \sim \sqrt{\Delta f}$. Since $S \sim P$, the laser-independent value to characterize the PA ADM is the normalized noise equivalent absorption coefficient (NNEA) determined as the minimum optical absorption coefficient (that is, resulting in S

TABLE I. Dimensions and Q factors in vacuum and air for three types of TFs. The dimensions are denoted as shown in Fig. 1, bottom.

	Dimensions, mm					
TF	ℓ	w	g	t	Q_{vac}	Q_{air}
1	3.8	0.58	0.30	0.30	87 000	13 000
2	3.8	0.58	0.20	0.24	126 000	12 000
3	2.8	0.30	0.20	0.10	116 000	8000

$=N$) multiplied by the optical excitation power and divided by the detector bandwidth. Lower NNEA means better ADM performance.

III. QUARTZ TUNING FORK: RESONANT PROPERTIES AND NOISE

TFs can be designed to resonate at any frequency in the 10–150 kHz range and beyond, but we assume below that a TF with $f_0=32\,768$ is used. So far, only the TFs with this resonant frequency were used in QEPAS experiments because of their ready commercial availability. Mechanical and electrical properties of TFs were extensively studied in relation with their application in ultrahigh resolution scanning microscopy pioneered by Karrai and Grober in 1995[8] (for latest developments see, e.g., Refs. 9–11 and references therein). The dimensions and several other TF parameters from three arbitrarily selected manufacturers are given in Table I, where the dimensions are denoted as shown in Fig. 1, bottom.

The mechanical and electrical properties of the TF are coupled via the piezoelectric effect. The TF parameters as a mechanical oscillator correspond to equivalent electrical parameters of a series *RLC* circuit: mass (m) to inductance (L), rigidity (k) to inverse capacity ($1/C$) and damping β to resistance R (Fig. 2, top). The resonant frequency f_0 and Q factor of the TF are related to R, L, and C as follows:

$$f_0 = \frac{1}{2\pi}\sqrt{\frac{k}{m}} = \frac{1}{2\pi}\sqrt{\frac{1}{LC}}, \tag{2}$$

$$Q = \frac{1}{R}\sqrt{\frac{L}{C}}. \tag{3}$$

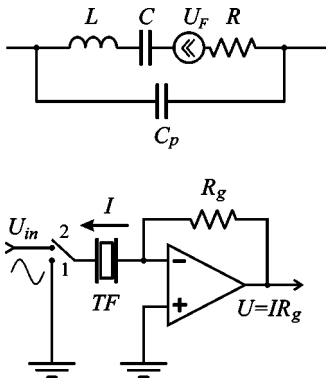

FIG. 2. Equivalent electric circuit of a TF (top). U_F is a voltage generated due to the action of the external mechanical force.[9] Schematic of the TF signal detection (bottom) for photoacoustic measurements (switch position 1) and the TF characterization (switch position 2).

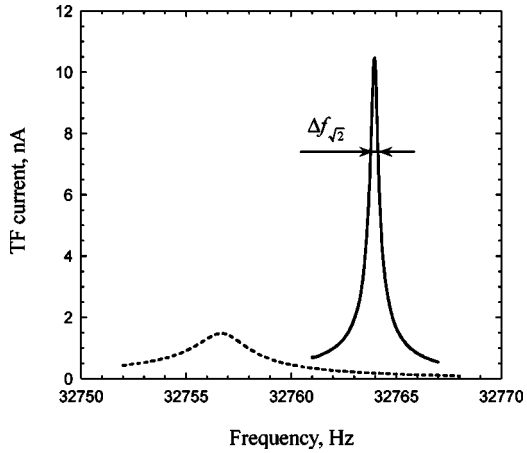

FIG. 3. The TF response to ac voltage ($V=140$ μV amplitude). The acquired curves yielded $Q=13\,271$ and $R=93.9$ kΩ at 755 Torr (dashed line); $Q=93\,456$ and $R=13.3$ kΩ in vacuum (solid line).

A mechanical deformation of the TF prongs induces electrical charges on its electrodes. A generally accepted way of observing the TF electrical response is to utilize a transimpedance amplifier as shown in Fig. 2 (bottom), switch position 1. A gain resistor $R_g=10$ MΩ was used in our design. Feedback maintains a zero voltage between the TF electrodes and thus the influence of the parallel stray capacitance C_p [Fig. 2(a)] is neutralized. In Ref. 12 it was shown that the TF noise in this circuit, measured at the amplifier output at the resonant frequency f_0, is equal to the thermal noise of the equivalent resistor R

$$\frac{\sqrt{\langle V_N^2\rangle}}{\sqrt{\Delta f}} = R_g\sqrt{\frac{4k_BT}{R}}, \tag{4}$$

where $\sqrt{\langle \Delta_N^2\rangle}$ is the rms voltage noise at the transimpedance amplifier output, Δf is the detection bandwidth, and T is the TF temperature. The gain resistor R_g also introduces noise with a spectral density $\sqrt{4k_BTR_g}$, but it is $\sqrt{R_g/R}$ times lower than the TF noise and can be usually neglected for typical values of $R\sim 10-100$ kΩ.

The electrical parameters of the TF can be determined by applying an ac voltage U to it as shown in Fig. 2 (bottom), switch position 2, and scanning frequency f of the applied voltage. The maximum of the $I(f)$ function, where I is the TF current and f is the modulation frequency of the applied voltage, yields f_0. In this manner, R and Q are determined using the two relations

$$R = \frac{U}{I(f_0)}, \quad Q = \frac{f_0}{\Delta f_{\sqrt{2}}}, \tag{5}$$

where $\Delta f_{\sqrt{2}}$ is the width of the $I(f_0)$ curve at the $I(f_0)/\sqrt{2}$ level (Fig. 3). The presence of the parallel C_p capacitance introduces a systematic error to measurements of the *RLC* circuit impedance. Typically $C_p\approx 2$ pf, and thus its impedance at $f_0=32.7$ kHz is $Z_C\approx 2.4$ MΩ and the $R\ll Z_C$ condition is satisfied. Therefore, the small error related to C_p can be neglected. Both f_0 and Q are dependent on the TF temperature, the surrounding gas pressure and the major chemical composition. Two resonant curves acquired for TF 1 (see Table I) in vacuum and when exposed to ambient atmosphere

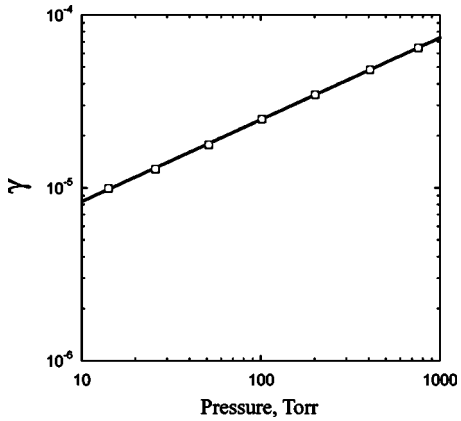

FIG. 4. Dependence of TF losses [see Eq. (6)] on air pressure.

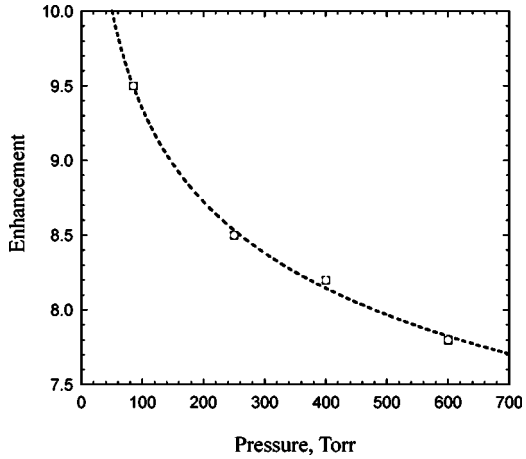

FIG. 5. Acoustic resonator enhancement factor ξ as a function of air pressure P. Experimental points are fitted with a curve: $\xi(P)=14.75P^{-0.1}$, where P is expressed in Torr.

are shown in Fig. 3. A number of studies on TF dampening in gases was reported in Refs. 9–16. All of them state a linear relation of f_0 and gas pressure P. However, there are some discrepancies regarding the Q dependence on P. For this reason we performed a characterization of the TFs used in this study at different gas pressures and composition. The linear nature of $f_0(P)$ was confirmed. For TF 1 the slope coefficient in air was found to be $df_0/dP=9.6\times10^{-3}$ Hz/Torr. To describe gas-induced vibration dampening we introduced a parameter γ defined as

$$\gamma=\frac{1}{Q}-\frac{1}{Q_{\mathrm{vac}}}, \tag{6}$$

where Q_{vac} is the TF Q factor in vacuum, which depends on internal losses in the TF as well as the losses added by the electrical circuit. It was found that $\gamma(P)=aP^b$ (Fig. 4), where a and b are parameters specific to a particular kind of TF. Thus, $Q(P)$ can be described as

$$Q=\frac{Q_{\mathrm{vac}}}{1+Q_{\mathrm{vac}}aP^b}. \tag{7}$$

For TF 1 in air $a=2.8\times10^{-6}$ and $b=0.47$, if P is expressed in Torr. We also studied the TF parameters in a mixture of air and SF_6. Both $f_0(c)$ and $\gamma(c)$ dependences were found to be linear as functions of SF_6 concentration c for a 0%–40% range

$$f_0(c)=f_0(0)-0.023c, \quad \gamma(c)=5.1\times10^{-7}c, \tag{8}$$

where c is expressed as a percentage, and $f_0(0)=32\,762.58$ Hz for studied TF 1.

IV. PHOTOACOUSTIC GAS SENSING WITH A TF: IMPLEMENTATION AND OBSERVATIONS

A. General principles

TFs with different dimensions including those listed in Table I were compared as QEPAS transducers without an additional acoustic resonator. It was found that the thickest of the tested TFs (1 in Table I) produced the highest signal-to-noise ratio (SNR) when photoacoustic sound was excited by a modulated laser beam focused between the TF prongs. Therefore TF 1 was selected as the transducer for all the gas-sensing studies as reported in this work.

To increase the effective interaction length between the radiation-generated sound and the TF, a half-wave acoustic resonator was installed. It consisted of two silica tubes, each 2.45 mm long with a 0.32 mm inner diameter, aligned perpendicular to the TF plane. The distance between the free ends of the tubes was equal to half wavelength of sound in air at 32.75 kHz, thus satisfying the resonant condition.[5] This resonator was found to enhance the QEPAS sensitivity ~8–10 times (Fig. 5), regardless of a ~0.4 mm wide gap between the tubes where the TF was located. The presence of the resonator did not noticeably change the measured Q factor of the TF. All the measurements described below were performed using an ADM consisting of the TF and such an acoustic resonator.

The QEPAS sensitivity to the concentration of the trace component in a specific gas sample is a function of the sample pressure. This dependence is determined by the following characteristic trends.

(1) TF Q-factor decreases at higher pressures [Eq. (7)]. From Eqs. (1), (3), and (4), it follows that the SNR is proportional to $\sqrt{Q}$ for a fixed f_0 and applied mechanical force.

(2) Peak optical absorption varies with pressure, especially at low (<30 Torr) pressures when the collisional line broadening is less than Doppler broadening. On the other hand, merging of closely spaced absorption lines should be taken into account at higher pressures.[17]

(3) Energy transfer from vibrationally excited molecules to translational degrees of freedom (V-T relaxation) is faster at higher pressures, resulting in more efficient sound excitation. The effect of the V-T relaxation rate on the PA signal is discussed in detail in Ref. 18.

(4) Acoustic resonator enhancement factor changes with pressure.

The laser wavelength modulation amplitude $\Delta\lambda$ must be optimized at each pressure for the highest $2f$ signal. The two-parameter optimization (pressure and $\Delta\lambda$) was reported for different gases in.[17–20] It was experimentally found that the optimum $\Delta\lambda\approx2\times$ full width at half maximum of the target absorption line.

The optical configuration of the QEPAS sensor should

TABLE II. Summary of published results on QEPAS based gas sensing. NNEA—normalized noise equivalent absorption coefficient. NEC—noise equivalent concentration for available laser power and $\tau=1$ s time constant.

Molecule (host) [Reference]	Frequency, cm^{-1}	Pressure, Torr	NNEA, $cm^{-1}\,W/Hz^{1/2}$	Power, mW	NEC ($\tau=1$ s), ppmv
NH_3 (N_2) 17	6528.76	60	7.2×10^{-9}	38	0.65
H_2O (exhaled air) 19	6541.29	90	8×10^{-9}	5.2	580
CO_2 (exhaled air) 19	6514.25	90	1.0×10^{-8}	5.2	890
N_2O (air+5%SF_6) 18	2195.63	50	1.5×10^{-8}	19	0.007
CO (N_2) 18	2196.66	50	5.3×10^{-7}	13	0.5
CO (propylene) 21	2196.66	50	7.4×10^{-8}	6.5	0.14
CH_2O (air) 20	2832.48	200	2.2×10^{-8}	3.4	0.55

be designed so as to avoid illumination of the TF and the inner surface of the enhancing acoustic resonator by the laser radiation, including any scattered light and incidental reflections from the optical elements. The $2f$ operation mode greatly reduces direct photothermal excitation of the TF. In particular, it was observed that the TF did not produce any electrical response even when ~2 mW of a 1.6 μm laser beam modulated at $f_0/2$ was directly focused to one of the TF prongs. However, temporal modulation of scattered and incidentally reflected radiation intensity is nonsinusoidal because of optical interference effects. Consequently, its modulation spectrum contains components at twice the modulation frequency and can excite the TF vibration. In the practical implementation of our QEPAS ADM the enhancing acoustic resonator mount serves as an efficient shield protecting the TF from the scattered radiation. Tilting the cell windows and the proper laser beam shaping resulted in background-free detection in all the gas-sensing experiments performed.

B. Review of published results on QEPAS-based trace gas sensors

The results reported so far in published QEPAS studies[17–21] are summarized in Table II. The first three table lines represent optical excitation in the overtone region, and the other four lines refer to the excitation of fundamental molecular vibrations. Comments on Table II follow.

NH_3 (Ref. 17): The NNEA measured for this molecule in the overtone region is the best among the tested species, pointing to fast vibrational-translational (*V-T*) relaxation of initially excited states. Signal dependence on the gas pressure follows the product of the peak absorption, TF *Q* factor, and acoustic resonator enhancement factor, which confirms that the $2\pi f_0\tau_{V\text{-}T}\ll1$ condition ($\tau_{V\text{-}T}$ is the *V-T* energy transfer time constant) is satisfied at gas pressures >30 Torr. The highest sensitivity was achieved at 60 Torr gas sample pressure.

H_2O and CO_2 (Ref. 19): The NNEA for both these molecules is close to the NEAA measured for NH_3, indicating a fast V-T relaxation of the excited states. However, minimum detectable concentration levels are high because the absorption lines within the tuning range of the available laser source are weak.

N_2O (Ref. 18): Addition of SF_6 to the sampled air promoted *V-T* relaxation and resulted in a 4 ppb NEC for $\tau=3$ s time constant.

CO in N_2 (Ref. 18): *V-T* relaxation of the fundamental vibration of this molecule is too slow for sound generation at 32.7 kHz. The observed QEPAS response is associated with fast rotational-translational relaxation of the rotational excitation accompanying absorption of the vibrational quantum.

CO in propylene, C_3H_6 (Ref. 21): A propylene host was found to promote *V-T* relaxation of CO to some extent. However, the speed of sound in propylene is different from air (or N_2). Hence the acoustic resonator tube length no longer satisfies the resonant condition. Furthermore, the lock-in amplifier phase was set to suppress the background propylene signal and therefore the phase did not necessarily coincide with the CO-originating photoacoustic signal.

CH_2O (Ref. 20): the SNR continued to grow slowly for pressures >200 Torr. However, selectivity requirements and laser wavelength modulation limitations did not allow us to acquire meaningful spectroscopic data at sample pressures beyond 200 Torr.

We can conclude from the above observations that the optimum pressure to detect molecules with isolated fast-relaxing optical transitions is ~50–90 Torr for the present ADM design. For slower relaxing species such as CH_2O the highest SNR is achieved at elevated gas sample pressures.

It was shown in Ref. 21 that the PA phase information can be used to enhance the chemical selectivity. This observation is not really unique to QEPAS but is relevant to PAS in general. However, PA operation at such high acoustic frequency as 32.7 kHz makes relaxation-related PA phase shifts more pronounced. Observation of PA phase shifts by means of a TF can be a powerful tool to study *V-T* relaxation processes in gases. As compared to the conventional PAS applied to relaxation studies, TF (when used without an enhancing acoustic resonator) offers advantages of resonant frequency and instrumental phase shift being practically independent of the gas pressure, temperature, and chemical composition.

C. Comparison with conventional PAS sensors and long-term stability

Among the seven species listed in Table II NH_3 exhibits the fastest *V-T* relaxation, which can be considered instantaneous on the $1/f_0$ time scale. Thus, the results for NH_3 monitoring permit the evaluation of the intrinsic QEPAS ADM sensitivity. A number of studies on trace ammonia detection by means of conventional PAS were reported, which allows a

TABLE III. Comparison of QEPAS NNEA with other published PAS sensors data.

Publication and comments	Resonant acoustic frequency, Hz	NNEA, $cm^{-1}\,W/\sqrt{Hz}$
[c]CO_2 laser, amplitude modulation	1840	1.1×10^{-8}
[d]Diode laser, amplitude modulation	4000	6.4×10^{-9}[a]
[b]Fiber-amplified diode laser, wavelength modulation	1800	2.2×10^{-9}[a]
Present work	32 760	5.4×10^{-9}

[a]Not as directly reported in the publication; see text for specific details.
[b]Reference 7.
[c]Reference 22.
[d]Reference 23.

comparison of QEPAS sensitivity with the results achieved by means of the conventional resonant PAS approach. For such a comparison, we selected three of the recent publications. Our latest result for NH_3 detection (obtained with the 6528.76 cm^{-1} absorption line) is NNEA $=5.4\times10^{-9}$ $cm^{-1}\,W/\sqrt{Hz}$. An improvement over the previously reported number (Ref. 17, see Table II) is due to an improved, tighter design of the enhancing acoustic resonator. Table III summarizes a comparative study of QEPAS and conventional PAS sensitivity, and detailed comments follow below.

Reference 22 described NH_3 detection using CO_2 laser radiation amplitude modulated at 1837 Hz and a resonant photoacoustic cell. The reported NNEA $=1.1\times10^{-8}$ $cm^{-1}\,W/\sqrt{Hz}$.

Another publication[23] described NH_3 detection with diode lasers amplitude modulated at 4 kHz and a differential resonant photoacoustic cell. The authors of Ref. 23 do not directly report NNEA or Δf values. However, they report that a sensitivity of 1.4×10^{-9} $cm^{-1}\,W$ was achieved with a $\tau=10$ s lock-in amplifier time constant. The lock-in amplifier equivalent noise bandwidth (ENBW, Ref. 24) depends also on a low-pass filter order. Assuming a first order filter (6 dB/oct), which gives the best NNEA, we measured directly the ENBW for the same lock-in amplifier (Stanford SR 830) and found that the ENBW $=0.048$ Hz. Substituting this for Δf, one obtains a NNEA $=6.4\times10^{-9}$ $cm^{-1}\,W/\sqrt{Hz}$.

The technique reported in Ref. 7 resembles the QEPAS sensor configuration. Wavelength modulated radiation was used for PA excitation, and the signal was detected at twice the modulation frequency. The resonant frequency of the PA cell was ~1800 Hz. The sensitivity reported in this work is an NNEA $=1.5\times10^{-9}$ $cm^{-1}\,W/\sqrt{Hz}$. However, as it can be derived from the presented data, the authors assumed $\Delta f=0.1$ Hz for a $\tau=10$ s lock-in amplifier time constant. This is most likely an error, since even a first order low-pass filter results in $\Delta f=0.048$ Hz, as mentioned in the previous paragraph. If such a correction is made, the sensitivity achieved in Ref. 7 is NNEA $=2.2\times10^{-9}$ $cm^{-1}\,W/\sqrt{Hz}$.

Hence, it can be concluded that the presently achieved QEPAS performance is higher than the reported results for amplitude modulation based resonant PAS [despite the much higher resonant frequency, which appears in the denominator of Eq. (1)], but is 2–3 times lower than wavelength-modulation based PAS sensors have achieved. This gap will most likely be closed with the future QEPAS developments. Specifically, a considerable gain in QEPAS sensitivity should be achieved when TFs with lower resonant frequencies are used [see Eq. (1)]. An added advantage of using a TF with a lower resonant frequency is more efficient photoacoustic sound generation in gas systems with low *V-T* relaxation rates, for example, formaldehyde in air.[20]

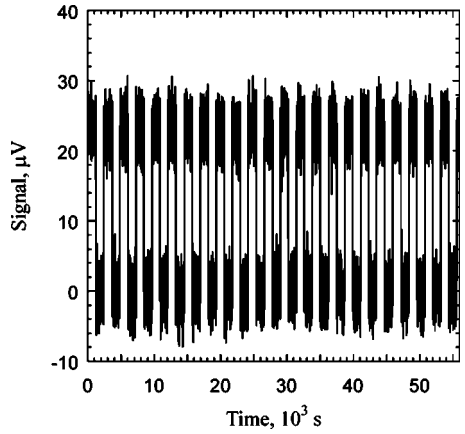

FIG. 6. Consecutive QEPAS readings acquired over a period of ~16 h. Nitrogen with 6 ppmv of NH_3 is supplied to the ADM, and the laser wavelength is alternatively switched to be on and off the NH_3 absorption line at 6528.4 cm^{-1}.

While NNEA describes the sensor performance on a short time scale, other kinds of measurements are required to characterize long-term drifts and establish the signal averaging limits. We shall follow the approach described in Ref. 25, which introduced utilization of Allan variance of time sequences of measurements to quantify the long-term stability of optical sensors. In order to obtain such statistical information, two kinds of data sets were acquired using the QEPAS NH_3 sensor described in Ref. 17.

(1) A flow of nitrogen with 6 ppmv (parts per million by volume) NH_3 from a trace gas standard generator was passed through the TF cell at a rate of 42 sccm. The gas pressure in the TF cell was maintained at 60 Torr by means of the pressure controller. The laser radiation was alternatively locked to the NH_3 absorption line at 6528.76 cm^{-1} (ON mode) or detuned to an absorption-free region at ~6528.4 cm^{-1} (OFF mode). ON and OFF modes were switched every 1200 s. As in Ref. 17, the laser power in the TF cell was 38 mW. The lock-in amplifier time constant was $\tau=1$ s, and third order low-pass filter settings (18 dB/oct) were used. With these settings of the lock-in amplifier the directly measured ENBW $=0.19$ Hz. The lock-in amplifier readings were recorded every 3 s, and the measurements performed continuously for ~16 h (Fig. 6). To perform an Allan variance analysis, all the data subsets with the laser on the absorption line were stacked together and treated as a single uninterrupted time sequence. A similar procedure was performed with the data subsets corresponding to the OFF mode.

(2) The laser beam was blocked, lock-in amplifier time constant changed to $\tau=0.3$ s (ENBW $=0.63$ Hz), and the

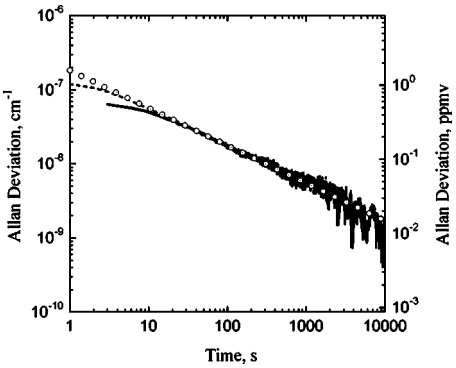

FIG. 7. Allan deviation as a function of the data averaging period. Solid line: laser is locked to the NH_3 absorption line at 6528.4 cm^{-1}, lock-in amplifier time constant 1 s. Dotted line: laser beam is blocked, lock-in amplifier time constant 0.3 s. Open circles trace $1/\sqrt{t}$ slope.

lock-in amplifier readings were recorded every 1 s. The total duration of this experiment was ~15 h.

The results of the Allan variance analysis are presented in Fig. 7. For clarity, Allan deviation ($\sqrt{\langle\sigma_A^2\rangle}$) is shown instead of the variance, and expressed in terms of absorption coefficient or ammonia concentration for this particular sensor. ON and OFF mode data resulted in practically coincident plots, therefore only the ON mode data are shown. The initial deviation of the curves from the $1/\sqrt{t}$ dependence is caused by the correlation of the lock-in amplifier readings for $\sim 8\tau$. The Allan deviation for all time sequences closely follows a $1/\sqrt{t}$ dependence over the entire duration of the measurements series. This observation verifies that white Johnson noise of the TF remains the dominant source of noise even on a multi-hour time scale, and the QEPAS based sensor allows practically unlimited data averaging without base line or sensitivity drift. For comparison, trace gas sensors based on direct optical absorption detection usually exhibit drifts that do not allow useful data averaging for time periods longer than 100–200 s (see, for example, Ref. 26).

The thermal stability of the QEPAS sensor has not been experimentally studied to date. However, it can be evaluated based on the known TF properties.[27] The resonant frequency f_0 of the tuning fork changes with temperature T according to the equation as specified in the TF data sheets

$$f_0(T) = f_0(25\ ^\circ\mathrm{C})[1 - 4 \times 10^{-8}(T - 25\ ^\circ\mathrm{C})^2]. \quad (9)$$

Hence, f_0 variation in the 5–45 °C range is ~0.5 Hz. This shift in resonant frequency is considerably smaller than $\Delta f_{\sqrt{2}} \approx 2.5$ Hz at atmospheric pressure and will cause only ~7% decrease in the detected signal if the laser modulation frequency is not adjusted accordingly. The decrease in the Q factor for the same ±20 °C temperature detuning from $T = 25$ °C is expected to be ~1%,[15] resulting in a proportional QEPAS signal change. Temperature changes are usually slow, and hence can be readily accounted for by periodic measurements of f_0 and Q and the respective adjustments of the laser modulation frequency and the normalization coefficient. Another temperature-related parameter is the resonant frequency of the enhancing acoustic resonator. The speed of sound in an ideal gas is proportional to the $\sqrt{T}$. So, a temperature variation of ±20 °C will cause ±3.5% variation in the acoustic resonator resonant frequency. The resulting change in the detected signal depends on the enhancing acoustic resonator Q factor and is more difficult to take into account than thermal changes in the TF properties. This problem is not specific to QEPAS but is general for resonant PAS. The resonant frequency of the gas-filled acoustic resonator is determined by its physical dimensions and therefore cannot be readily changed. Hence if the QEPAS sensor is required to operate over a wide range of temperatures its sensitivity should be pre-calibrated in this range. An alternative approach can be to have a set of ADMs optimized for different temperatures and direct the laser radiation to a specific ADM depending on the gas temperature. The small size of the QEPAS ADM and the availability of compact microelectromechanical system optical switches make such an approach feasible.

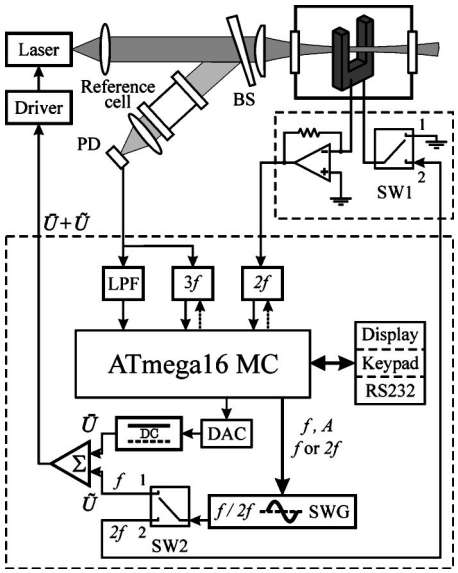

FIG. 8. Functional diagram of the QEPAS based gas sensor. PD—photodetector, BS—beamsplitter, SW1 and SW2—electronic switches, LPF—low-pass filter, MC—microcontroller, DAC—digital-analog converter, SWG—sine wave generator

V. AUTONOMOUS QEPAS BASED CHEMICAL SENSOR ARCHITECTURE

The response speed of the QEPAS technique is intrinsically limited. The oscillator relaxation time constant is $\tau_r = Q/\pi f_0$ (see, e.g., Ref. 27). For a typical $Q \sim 30\,000$ at 50 Torr and $f_0 = 32.76$ kHz, $\tau_r \approx 0.3$ s. Hence, to detect the signal within 5% of its steady-state value we should sample not more often than approximately once a second. Therefore, it is not practical to configure a QEPAS based chemical sensor for spectral scans of an absorption line. Instead, the laser wavelength must be locked to the target absorption line center. This approach is justified because of the background-free nature of $2f$ QEPAS, which was experimentally confirmed repeatedly.

The functional diagram of the QEPAS based autonomous chemical gas sensor is shown in Fig. 8. The sensor utilizes a $2f$ wavelength-modulation spectroscopy approach, where $2f = f_0$ in the case of QEPAS. The sensor consists of

the three subsystems: a control and data processing electronics unit (CEU) schematically shown as a large dashed box in Fig. 8, a transimpedance amplifier with an electronic switch shown as a small dashed box (this unit has to be positioned close to the TF), and a set of optical components including the excitation laser, reference cell with a photodetector, and a TF. The optical components can vary depending on the spectral range, target molecule and the excitation laser. It is assumed that the laser wavelength is determined by the voltage applied to the laser driver input. For example, the wavelength of a distributed feedback semiconductor laser changes with current. Hence the current source with an analog voltage input can be used as the "Driver" in Fig. 8. The dc component of the laser driver input $\overline{U}$ determines the laser central wavelength, while the ac component $\tilde{U}$ provides the wavelength modulation.

The CEU is based on an ATmega16 microcontroller (MC, Atmel Corporation) and has two primary modes of operation: the measurement mode and the calibration mode. In the measurement mode the switches SW1 and SW2 are in position 1, and the following functions are performed:

(1) sine wave generator SWG generates a sine wave $\tilde{U}$ at $f=\frac{1}{2}f_0$. Amplitude A and frequency f are controlled by the MC;
(2) the laser power (dc component of the photodetector (PD) signal) is measured;
(3) the $3f$ component of the PD signal is measured and the $\overline{U}$ is adjusted proportionally to maintain the laser wavelength at the center of the absorption line; and
(4) the S (TF signal amplitude) is measured by the $2f$ lock-in amplifier channel. Measurement and digitization accuracy are sufficient for TF thermal noise detection.

The CEU is normally programmed to switch to the calibration mode every 30 min. This mode can also be initialized manually or via RS232 interface. The calibration lasts ~3 min and consists of the following operations:

(1) TF parameters f_0 and Q are measured and stored in the CEU memory. In order to perform this function switches SW1 and SW2 are set to position 2. The sine wave generator (SWG) is switched to the $2f$ mode, and the frequency $2f$ is scanned encompassing f_0. The maximum position and the width of the TF response $S(2f)$ are used for f_0 and Q calculations, respectively;
(2) SWG is switched back to the f mode with the updated f value;
(3) laser wavelength is adjusted in the same manner as operation (3) of the measurement mode; and
(4) the background level is measured. To perform this operation a pre-set voltage ΔU is added to $\overline{U}$ to detune the laser from the target absorption line, and the background signal S_b is measured and stored in the CEU memory.

The TFs used in QEPAS so far are resonant at ~32.76 kHz, but the CEU can be configured to accommodate 20 and 10 kHz crystals. The external dimensions of the current version of the CEU case are $(23\times16\times10)$ cm, including a built-in power supply. To make the CEU an integral part of the QEPAS gas sensor, the initial parameters such as the $\overline{U}$ level, the $\tilde{U}$ amplitude and phase, and feedback coefficient for line locking must be set. This can be performed either from the front-panel keypad or via a RS232 serial interface. Parameters are stored in the CEU memory. A two-line liquid crystal display indicates the current operation parameters including the updated $\overline{U}$ value and the mode of operation ("calibration" or "measurement"), as well as the most important measured values such as the Q factor, f_0, laser power, and S. A LABVIEW driver was created for convenient initial setup and laboratory tests. The CEU was tested for C_2H_2 detection with 32.76 and 20.0 kHz TFs (without acoustic resonator). The CEU performance was found to equal the performance of the laboratory setup which incorporated two commercial lock-in amplifiers (SR 830 DSP, Stanford Research Systems) and a computer-controlled function generator (DS 345, Stanford Research Systems). The measured noise level matched the theoretically calculated TF noise within 10% accuracy.

ACKNOWLEDGMENTS

The authors gratefully acknowledge financial support from the National Aeronautics and Space Administration, the Texas Advanced Technology Program, the Robert Welch Foundation, and the Office of Naval Research via a subaward from Texas A&M University. The authors acknowledge Chad Roller for his input in the Allan variance analysis of time series.

[1] R. F. Curl and F. K. Tittel, Annu. Rep. Prog. Chem., Sect. C: Phys. Chem. **98**, 219 (2002).
[2] F. Capasso, C. Gmachl, R. Paiella, A. Terdicucci, A. L. Hutchinson, D. L. Sivco, J. N. Baillargeon, A. Y. Cho, and H. C. Liu, IEEE J. Sel. Top. Quantum Electron. **6**, 931 (2000).
[3] R. Q. Yang, J. L. Bradshaw, J. D. Bruno, J. T. Pham, and D. E. Wortman, IEEE J. Quantum Electron. **38**, 559 (2002).
[4] V. P. Zharov and V. S. Letokhov, *Laser optoacoustic spectroscopy*, Springer Series in Optical Sciences Vol. 37 (Springer, Berlin, 1986).
[5] A. Miklós, P. Hess, and Z. Bozóki, Rev. Sci. Instrum. **72**, 1937 (2001).
[6] A. A. Kosterev, Yu. A. Bakhirkin, R. F. Curl, and F. K. Tittel, Opt. Lett. **27**, 1902 (2002).
[7] M. E. Webber, M. Pushkarsky, and C. K. N. Patel, Appl. Opt. **42**, 2119 (2003).
[8] K. Karrai and R. D. Grober, Appl. Phys. Lett. **66**, 1842 (1995).
[9] D. V. Serebryakov, A. P. Cherkun, B. A. Loginov, and V. S. Letokhov, Rev. Sci. Instrum. **73**, 1795 (2002).
[10] T. Akiyama, U. Staufer, N. F. de Rooij, P. Frederix, and A. Engel, Rev. Sci. Instrum. **74**, 112 (2003).
[11] A. P. Cherkun, D. V. Serebryakov, S. K. Sekatskii, I. V. Morozov, and V. S. Letokhov, Rev. Sci. Instrum. (submitted).
[12] R. D. Grober, J. Acimovic, J. Schuck, D. Hessman, P. J. Kindlemann, J. Hespanha, A. S. Morse, K. Karrai, I. Tiemann, and S. Manus, Rev. Sci. Instrum. **71**, 2776 (2000).
[13] M. Christen, Sens. Actuators **4**, 555 (1983).
[14] H. Itoh, Proceedings of the 2002 IEEE International Frequency Control Symposium & PDA Exhibition, New Orleans, Louisiana, 29–31 May, 2002, pp. 744–755.
[15] H. Hojoh, US Patent No. 4,741,213 (1988).
[16] L. N. Liebermann and P. Salzmann, US Patent No. 5,136,885 (1992).
[17] A. A. Kosterev and F. K. Tittel, Appl. Opt. **43**, 6213 (2004).
[18] A. A. Kosterev, Y. A. Bakhirkin, and F. K. Tittel, Appl. Phys. B: Lasers Opt. **80**, 133 (2005).
[19] D. Weidmann, A. A. Kosterev, and F. K. Tittel, Opt. Lett. **29**, 1837 (2004).
[20] M. Horstjann, Y. A. Bakhirkin, A. A. Kosterev, R. F. Curl, and F. K. Tittel,

Appl. Phys. B: Lasers Opt. **79**, 799 (2004).
[21] A. A. Kosterev, Y. A. Bakhirkin, F. K. Tittel, S. Blaser, Y. Bonetti, and L. Hvozdara, Appl. Phys. B: Lasers Opt. **78**, 673 (2004).
[22] M. B. Pushkarsky, M. E. Webber, and C. K. N. Patel, Appl. Phys. B: Lasers Opt. **77**, 381 (2003).
[23] A. Schmohl, A. Miklós, and P Hess, Appl. Opt. **41**, 1815 (2002).
[24] A. Mandelis, Rev. Sci. Instrum. **65**, 3309 (1994).
[25] P. Werle, R. Mücke, and F. Slemr, Appl. Phys. B: Photophys. Laser Chem. **57**, 131 (1993).
[26] B. P. Wert, A. Fried, S. Rauenbuehler, J. Walega, and B. Henry, J. Geophys. Res. **108**, 4350 (2003).
[27] T. L. Chow, *Classical Mechanics* (Wiley, New York, 1995).